CrossMark

ORIGINAL ARTICLE

Using small triangular baffles to facilitate upstream fish passage in standard box culverts

Joseph Cabonce[1] · Ramith Fernando[1] · Hang Wang[1] · **Hubert Chanson[1]**

Abstract A culvert is a covered channel to pass streams and floodwaters through an embankment. The ecological impact of culverts has been recognised, in particular in terms of stream connectivity, but existing guidelines lead often to un-economical culvert design. Herein, a small triangular corner baffle system was tested physically in a near-full-scale fish-friendly facility of a box culvert barrel. Experiments were repeated with several configurations to characterise the flow properties for a range of less-than-design flows, baffle sizes and spacings. In presence of triangular corner baffles, the flow was asymmetrical, owing to the wake behind each baffle. The presence of triangular corner baffles had a moderate effect on the flow resistance and discharge capacity, albeit the data indicated the combined effect of relative baffle height and spacing on the friction factor. With triangular baffles, the surface area of slow velocity regions increased by a factor of two to three. Such low velocity regions are preferential swimming zones for fish, beneficial to small-bodied fish passage. Testing with small-bodied fish showed that fish preferred to swim upstream in slow-velocity regions, typically next to the sidewalls and in the left corner where the triangular baffles were located. The presence of small triangular baffles facilitated substantially the upstream passage of small fish, including in terms of endurance, compared to a smooth un-baffled box culvert barrel, when the baffle size was comparable to the fish length. The present findings highlighted the importance of physical modelling at near full-scale for the development of fish-friendly culvert designs.

Keywords Box culverts · Fish passage · Triangular baffles · Hydrodynamics · Boundary shear stress · Physical modelling · Low velocity zones (LVZs)

Abbreviations
PVC   Polyvinyl chloride
s   Second

✉ Hubert Chanson
   h.chanson@uq.edu.au

1   The University of Queensland, School of Civil Engineering, Brisbane, QLD 4072, Australia

h   Hour
min   Minute

List of symbols
B   Channel width (m)
D_H Hydraulic diameter (m)
d   Water depth (m)
d_c Critical flow depth (m)
d_1 Inflow depth (m)
Fr   Froude number; for a rectangular channel: $Fr = \dfrac{V}{\sqrt{g \times d}}$

f   Darcy–Weisbach friction factor
f_{skin} Skin friction factor measured with a Prandtl–Pitot tube lying on the bed
f′   Skin friction factor
g   Gravity acceleration (m/s^2): g = 9.794 m/s^2 in Brisbane, Australia
H   Internal barrel height (m)
h_b Triangular baffle height (m)
K   Head loss coefficient
k_s Equivalent sand roughness height (m)
L   Channel length (m)
L_b Longitudinal spacing (m) between baffles
L_t Turbulent length scale (m)
l_m Mixing length (m)
Mo   Morton number
N   Velocity power law exponent
Q   Water discharge (m^3/s)
Q_{des} Design discharge (m^3/s) of culvert structure
P   Pressure (Pa)
R   Normalised correlation coefficient
Re   Reynolds number defined in terms of the hydraulic diameter: $Re = \rho \times V_{mean} \times D_H / \mu$
S_o Bed slope: $S_o = \sin\theta$
T_t Turbulent time scale (s)
V   Flow velocity (m/s) positive downstream
V_b Velocity (m/s) measured by a Pitot–Prandtl–Preston tube lying on the bed
V_c Critical flow velocity (m/s)
V_{fs} Free-surface velocity (m/s)
V_{max} Maximum velocity (m/s); free-stream velocity (m/s) above boundary layer
V_{mean} Cross-sectional mean velocity (m/s): $V_{mean} = Q/(B \times d)$; also called bulk velocity
V_1 Inflow velocity (m/s)
V_x Longitudinal velocity component (m/s)
V′   Velocity fluctuation (m/s)
X   Relative distance between baffles: $X = (x - x_b)/L_b$
x   Longitudinal distance (m) positive downstream
x_b Longitudinal baffle position (m)
Y_{Vmax} Transverse distance (m) where $V_x = (V_{max})_M$
y   Transverse distance (m) measured from the right sidewall positive towards the left
            sidewall
Z_{Vmax} Vertical elevation (m) where $V_x = V_{max}$
z   Vertical distance (m) positive upwards with z = 0 at the invert

z_b	Elevation (m) of Prandtl–Pitot tube dynamic tapping when the tube is lying on the bed
ΔH	Manometer reading (m)
δ	Boundary layer thickness (m)
κ	von Karman constant: $\kappa = 0.4$
μ	Dynamic viscosity (Pa.s) of water
ν_T	Eddy viscosity (m²/s)
θ	Angle between bed slope and horizontal
ρ	Water density (kg/m³)
σ	Surface tension (N/m) between air and water
τ_o	Skin friction boundary shear stress (Pa)
$\emptyset$	Diameter (m)

Subscripts

M	Cross-sectional maximum value
max	Maximum value in a vertical profile
skin	Skin friction
x	Longitudinal direction positive downstream
1	Upstream flow conditions

1 Introduction

A culvert is a covered channel of relatively short length designed to pass streams and floodwaters through or beneath an embankment (Fig. 1). Current designs are very similar to ancient designs [7, 33]. They are characterised by some significant afflux at design flows [8, 20]. The afflux is the rise in the upstream water level caused by the presence of the culvert and it is a quantitative measure of the upstream flooding induced by the culvert structure. During the last four decades, the ecological impact of culverts has been recognised, in particular in terms of stream connectivity [3, 10]. Guidelines were developed to provide for upstream fish passage, too often leading to un-economical culvert designs [15, 23]. In terms of hydraulic engineering, the optimum size of a culvert is the smallest barrel size allowing for inlet control operation [8, 18, 21]. Hydrological and hydraulic engineering considerations often yield large velocities in the barrel, creating an upstream fish passage barrier. In some cases, baffles may be installed along the barrel invert to provide a fish-friendly alternative [5, 34, 44]. Unfortunately, most baffles can reduce drastically the culvert discharge capacity for a given afflux [24, 34].

Hydraulic design guidelines rarely consider non-design flow conditions ($Q < Q_{des}$), but fish swim during all flow conditions for $Q > 0$, where Q is the water discharge and Q_{des} is the culvert design discharge. Herein, a simple triangular corner baffle system is proposed for less-than-design discharges, creating slow flow regions, suitable to assist small bodied fish passage. The design derives from initial tests in a small-size culvert model [44]. The small corner baffle system was tested systematically in a near-full-scale culvert barrel flume with a fish-friendly water recirculation system. Experiments were conducted with several configurations to ascertain potential scale effects as well as to quantify the effects of baffle size and spacing.

Fig. 1 Box culvert operation. **A** Box culvert outlet on 30 March 2017—stream; Whitton Creek, Brisbane QLD (Australia)—flow direction from background to foreground. **B** Box culvert inlet operation on 31 March 2017 for less-than-design flow conditions—stream: Caswell Creek, Canungra QLD (Australia)—flow direction from background right to foreground left

2 Physical modelling

2.1 Presentation

In experimental fluid mechanics, a model study of a prototype structure is to provide reliable predictions of the flow properties of the prototype structure [16, 32]. Any physical study is based upon the basic concept and principles of similitude, to ensure a reliable and accurate extrapolation of the model results to the prototype. The processing, analysis and interpretation of experimental data constitutes an essential component in physical modelling [13], and dimensional analysis is the basic procedure to deliver the relevant dimensionless parameters. For any dimensional analysis of fish swimming in a culvert, the relevant dimensional parameters include the fluid properties, physical

constants, channel geometry, initial flow conditions, turbulent flow conditions as well as fish properties including fish dimensions and specie. Recent results suggested that a complete similarity between laboratory data and prototype observations may be unattainable, unless working at full scale or near full-scale [42]. Herein, the experiments were conducted in a large-size facility operating at relatively large Reynolds numbers: $Re > 2 \times 10^5$ (Fig. 2). The channel corresponded to a small box culvert barrel cell (e.g. Fig. 1B), or to a 1:5 scale model of a single cell for the large structure seen in Fig. 1A.

2.2 Experimental facility and instrumentation

New experiments were conducted at the University of Queensland. Measurements were conducted in a 12 m long 0.5 m wide rectangular tilting flume representing a single box culvert barrel cell. The channel bed was horizontal herein ($S_o = 0$): the horizontal slope was selected
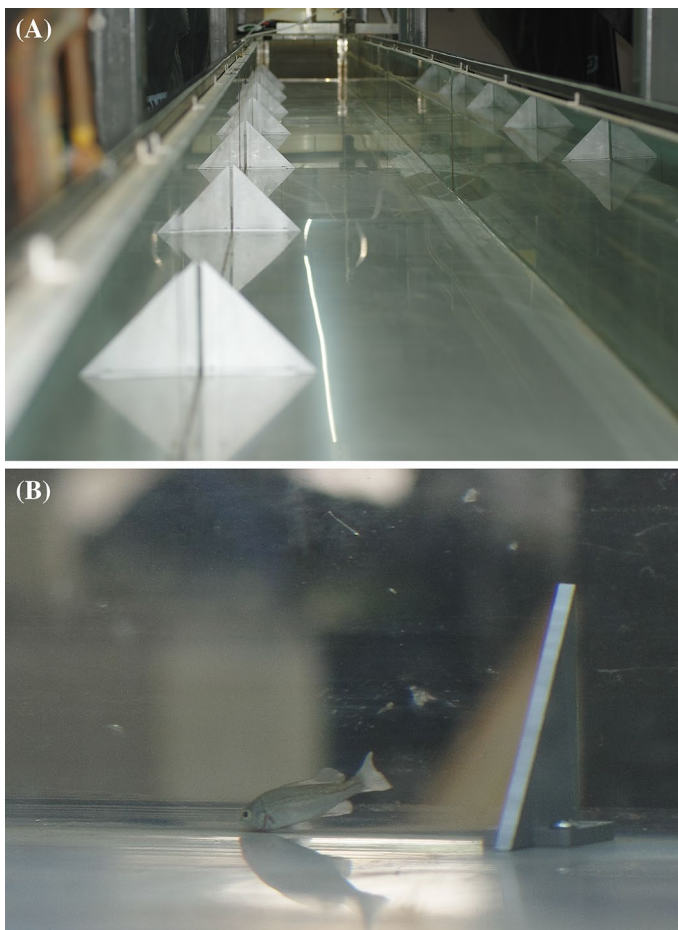

Fig. 2 Experimental channel. **A** Dry channel with triangular corner baffles ($h_b = 0.133$ m, $L_b = 1.33$ m). **B** Channel operation with a juvenile silver perch (*Bidyanus bidyanus*) resting in the stagnation zone upstream of a triangular corner baffle—flow conditions: Q = 0.0556 m³/s, $h_b = 0.067$ m, $L_b = 0.67$ m, flow direction from left to right

to reduce the number of independent variables. The flume was made of smooth PVC bed and glass walls (Fig. 2). The waters were supplied by a constant head tank feeding a large intake basin leading to the test section through a series of flow straighteners, followed by convergent bottom and sidewalls. Stainless steel screens were installed at both upstream and downstream ends to ensure the safety of small fish, e.g. seen in Fig. 2B.

The water discharge was supplied by a constant head reticulation system, equipped with a biological filter system, enabling fish-friendly chemical-free water. The flow rate was measured with an orifice meter that was designed based upon the British Standards and calibrated on site. The percentage of error was expected to be less than 2%. The water depths were measured using rail mounted pointer gauges with an accuracy of ± 0.5 mm. Velocity and pressure measurements were conducted with a Dwyer® 166 Series Prandtl–Pitot tube, with a 3.18 mm diameter tube, a hemispherical total pressure tapping ($\varnothing = 1.19$ mm) at the tip and four equally spaced static pressure tappings ($\varnothing = 0.51$ mm) located 25.4 mm behind the tip. The translation of the Prandtl–Pitot probe in the vertical direction was controlled by a fine adjustment travelling mechanism connected to a Mitutoyo™ digimatic scale unit, with an error $\Delta z < \pm 0.025$ mm. The accuracy on the longitudinal position was estimated as $\Delta x < \pm 2$ mm. The accuracy on the transverse position of the probe was less than 1 mm. The experiments were documented using a digital SLR camera Pentax™ K-3. Further details were reported in Cabonce et al. [4].

2.3 Calibration of Prandtl–Pitot tube

The Prandtl–Pitot tube was calibrated to measure the skin friction shear stress when the tube was in contact with the wall. The concept is based upon basic theoretical considerations (Appendix A). The calibration was herein conducted in open channel flows and yielded a monotonic relationship between the boundary shear stress and Prandtl–Pitot tube reading (Fig. 3). The result followed closely a solution of the Prandtl mixing length model in the wall region:

$$\tau_o = \rho \times \kappa^2 \times \frac{V_b^2}{N^2} \tag{1}$$

Fig. 3 Calibration curve of Prandtl–Pitot tube for skin friction boundary shear stress—comparison with Eq. (1) assuming $N = 7$ and the correlations of Patel [35] in wind tunnels and Macintosh [27] in open channels, and with the experimental calibration of Chanson [6] in open channel
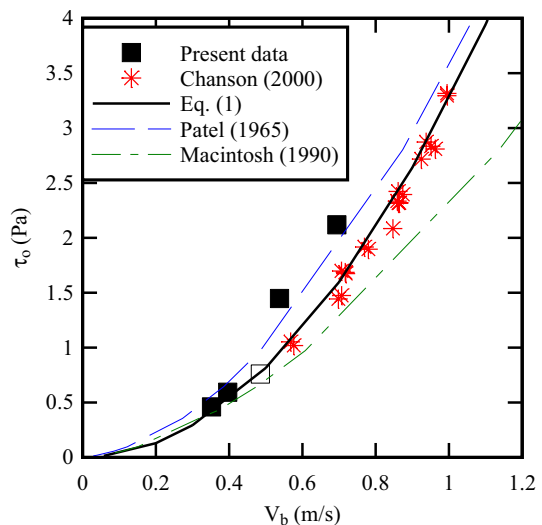
where τ_o is the local skin friction boundary shear stress, ρ is the fluid density, κ is the von Karman constant ($\kappa = 0.4$), N is the power law exponent and V_b is the velocity measured by the Prandtl–Pitot tube lying on the boundary. The theoretical solution (Eq. (1)) is close to present calibration data as well as previous calibration curves obtained in wind tunnels and open channels as seen in Fig. 3.

The Prandtl–Pitot tube was also calibrated in negative flow regions. When the velocity was negative, the dynamic tapping was in the wake of the tube and the dynamic head became smaller than the static head. Darcy [12] pioneered the usage of a tube facing downstream to record some depression [40]. Further studies developed instruments with a pressure tapping located in a wake region [22, 27, 28]. Despite some data scatter caused by the very small pressure difference between the total and static tappings, the velocity and head difference were herein correlated by:

$$V_x = -17.81 \times (-\Delta H)^{0.538} \qquad (2)$$

where V_x is the (negative) velocity in m/s, ΔH is the difference between the total head and piezometric head in m, and the normalised correlation coefficient was $R = 0.801$.

2.4 Fish testing

Fish swimming observations were conducted using juvenile silver perch (*Bidyanus bidyanus*). Fish were fasted for 24 h before being tested at 24.5 ± 0.5 °C. Fish were placed for 5 min in a pervious containment, installed in the running flume. The short conditioning phase allowed the fish to adjust to the flow and channel shape. After 5 min, the pervious containment box was removed, and the fish were released, typically travelling upstream. Recording began after a 2 min acclimation period and fish kinematics was recorded for 15 min. If a fish showed signs of fatigue, the test would be stopped and the fish removed from flume. In this study, fish were selected randomly for each experiment, and each fish was tested once only. All experimentation was conducted with the approval of The University of Queensland Animal Ethics Committee (Certificate no. SBS/312/15/ARC).

The positions of fish were recorded manually and with video cameras using a 3-D grid scale based upon the boundary roughness square pattern. The manual observations and video recordings yielded close results. All recordings showed that the fish spent most time in a reasonably thin vertical layer close to the sidewalls, in particular the left sidewall corner for the triangular baffle configurations. In addition, high-resolution photographs were taken with a Pentax™ K-3 dSLR camera equipped with prime lenses with negligible lens distortion. Swimming performance was quantified as the ability to complete the 17 min fixed flow rate trial, categorised as success or failure, and the time to fatigue for those that failed.

2.5 Experimental flow conditions

Several boundary configurations were tested. Reference experiments were performed with the smooth PVC invert and smooth sidewalls (Smooth Boundary). Further experiments were conducted with several types of isosceles triangular baffle configurations (Fig. 2), following the preliminary observations of Wang et al. [44]. The triangular baffles were fixed in the bottom left corner of the flume (Fig. 2A). Each baffle was an isosceles triangle with a 45° angle. Three different sizes and six different longitudinal spacings were tested, with a constant baffle size and spacing for the whole channel length (Table 1, Fig. 2A). Herein, the baffle size range was selected to be comparable to the targeted fish specie dimensions.

Table 1 Experimental investigations of box culvert barrel flows

References	Barrel dimensions	Q (m³/s)	Boundary configurations	Instrument(s)
Present study	B = 0.50 m L = 12 m	0.0261–0.0556	Smooth boundary Triangular baffles h_b = 0.033, 0.067, 0.133 m L_b = 0.33, 0.67, 1.0, 1.33, 1.66, 2.0 m	Pointer gauge
		0.0261	Smooth boundary Triangular baffles h_b = 0.067 m, L_b = 0.67 m h_b = 0.133 m, L_b = 1.33 m	Pointer gauge and Prandtl–Pitot tube
		0.0556	Smooth boundary[a] Triangular baffles h_b = 0.067 m, L_b = 0.67 m[a] h_b = 0.133 m, L_b = 0.67 m[a] h_b = 0.133 m, L_b = 1.33 m	
Wang et al. [44]	B = 0.150 m H = 0.105 m L = 0.50 m	0.001–0.014	Smooth boundaries Rough invert (P40 and P60 sandpaper) Diagonal baffles (h_b = 0.012 m, L_b = 0.100 m) Streamlined diagonal baffles (h_b = 0.012 m, L_b = 0.100 m) Corner baffles (h_b = 0.020 m, L_b = 0.100 m) Partial pipe	Pointer gauge
	B = 0.50 and 0.478 m L = 12 m	0.0261 0.0556	Config. 1: smooth boundaries Config. 2: rough invert and smooth sidewalls Config. 3: rough invert and rough left sidewall	Pointer gauge and acoustic Doppler velocimeter

B: internal channel width; H: internal barrel height; h_b: baffle height; L: channel test section length; L_b: longitudinal baffle spacing; Q: discharge

[a]Fish testing

Previous studies showed indeed that fish performances may be functions of the ratio of vortex size to fish length [45], with fish performing best when the coherent structure sizes were similar to the fish dimensions [29, 41].

Several series of experiments were conducted for flow conditions corresponding to less-than-design discharges with a cross-sectional averaged velocity $V_{mean} < V_c$, where V_{mean} is the cross-sectional averaged velocity: $V_{mean} = Q/(B \times d)$ and V_c is the critical flow velocity: $V_c = (g \times Q/B)^{1/3}$, with g the gravity acceleration and B the channel width. Table 1 summarises the experimental conditions, including a comparison with a previous study. Free-surface measurements and dye injection observations were conducted for all triangular baffle configurations. Detailed velocity measurements were performed with a narrower range of boundary conditions and flow rates (Table 1).

3 Basic flow patterns

At the upstream end of the culvert barrel flume, the flow was quasi-uniform. With increasing longitudinal distance, bottom and sidewall boundary layers developed. In the smooth boundary configuration, the outer edge of the developing boundary layer interacted with the free-surface for $x > 4$–6 m depending upon the flow rate, where x is the longitudinal co-ordinate positive downstream and $x = 0$ at the upstream end of the flume. With the triangular baffle boundary configurations, the first baffle being located at $x \sim 0.5$ m, the flow became fully three-dimensional as a result of the turbulence generated by the baffles for $x > 4$ m. In the followings, the experimental observations focused on the fully-developed flow region, i.e. $x > 6$ m.

For all flow conditions, the water flow was subcritical ($V_{mean} < V_c$) and the free-surface was relatively smooth. The water depth decreased with increasing longitudinal distance, typical of a H2 backwater profile. For the largest baffles ($h_b = 0.133$ m) and all longitudinal baffle spacings, the free-surface presented some localised dip immediately downstream of each baffle next to the left sidewall (Fig. 4). It is believed to be linked to local flow separation in the near-wake of the baffle, associated with a local fluid acceleration and associated pressure reduction, according to ideal-fluid flow theory. The noticeable dip indicated some localised energy dissipation linked to major flow redistributions induced by the baffles.

Recirculation visualisations using dye injection were conducted for 4.5 m < x < 8.1 m. Visual observations showed clearly the flow separation taking place at each baffle outer edge, with a region of local flow acceleration, a shear zone and recirculation region in the wake of the baffle. Several flow features were identified between successive baffles, as sketched in Fig. 4.

The bulk of the flow took place for $y/(B - h_b) < 1$, where y is the transverse distance measured from the right sidewall. No recirculation or flow reversal was observed, including next to the right smooth sidewall, opposite to the baffle side. At the inclined edge of the triangular baffle, flow separation took place and a shear zone developed immediately downstream (Fig. 4). In the shear zone, momentum was transferred from the high velocity region to the recirculation region behind the baffle. Behind each baffle, a sizeable zone of flow reversal was observed, where the water flowed in the negative direction. Such a recirculation region may serve as rest areas for fish [5, 34], although strong recirculation might have detrimental effect on small fish passage, with fish being affected by the sudden change in flow direction (see below). The recirculation region height was about the baffle size h_b, and its length was of the order of three baffle heights ($3 \times h_b$). Downstream of the recirculation region, a re-attachment region was characterised by a highly turbulent motion
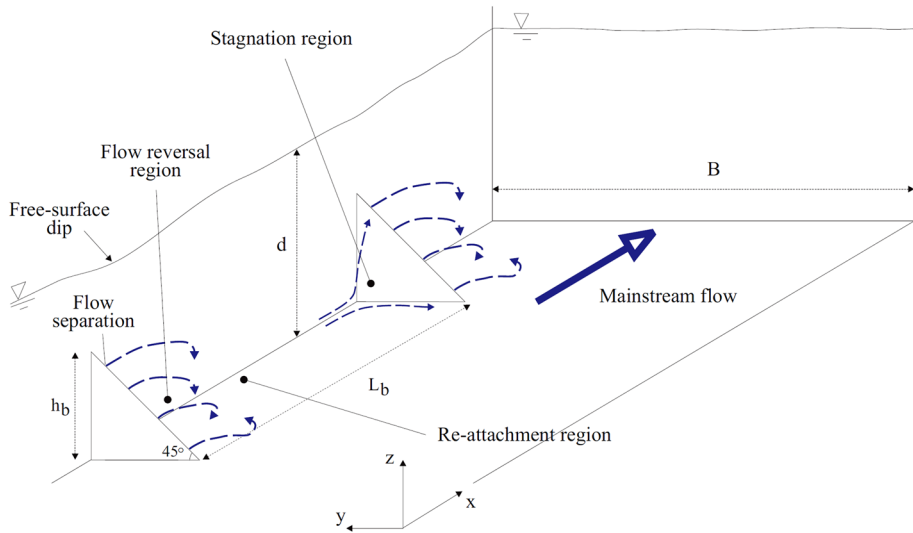
Fig. 4 Flow patterns and recirculation motion between two successive baffles along the left sidewall

with a mean velocity about zero. The length of this re-attachment region was of the order of a baffle height (h_b). Further downstream and immediately upstream of the next baffle, a relatively small stagnation region was observed (Fig. 4). This region was characterised by a change in fluid direction, as the streamlines spread around the baffle. Locally the fluid velocity was small. Visual observations showed that small fish could use the stagnation region as a rest zone (Fig. 2B). Overall visual observations suggested that the flow velocity and baffle spacing had no visible effect on the overall recirculation pattern. The baffle size mostly increased the flow reversal region, particularly its longitudinal size, while the stagnation region became more pronounced for the largest baffle size.

The flow resistance of triangular baffle boundary configurations was tested and compared to the smooth channel results. The spatially-averaged boundary shear stress was deduced from the measured free-surface profiles and slope of the total head line (i.e. friction slope) in the fully-developed flow region ($x > 6$ m) with an uncertainty about 5%. The results are presented in dimensionless form in terms of Darcy–Weisbach friction factor. Study results are reported in Fig. 5, where D_H is the hydraulic diameter and Re is the Reynolds number defined in terms of the cross-sectional averaged velocity V_{mean} and hydraulic diameter D_H. In Fig. 5A, the present data are compared to the Karman-Nikuradse formula for smooth turbulent flows [38] and to the data of Wang et al. [44]. The smooth boundary configuration data were in close agreement with smooth turbulent theoretical results, while the data with the largest relative baffle heights compared favourably with the rough wall configuration data of Wang et al. [44] in the same flume. Figure 5B illustrates the combined effect of relative baffle height h_b/D_H and relative baffle spacing h_b/L_b. Simply, the data showed an increasing friction factor with increasing relative baffle height for a given ratio h_b/L_b. The flow resistance further increased with increasing ratio h_b/L_b for a constant relative baffle height h_b/D_H.

Overall the presence of triangular baffles had a moderate effect on the flow resistance. The Darcy-Weibach friction factor data for the triangular corner baffle channel were best correlated by:
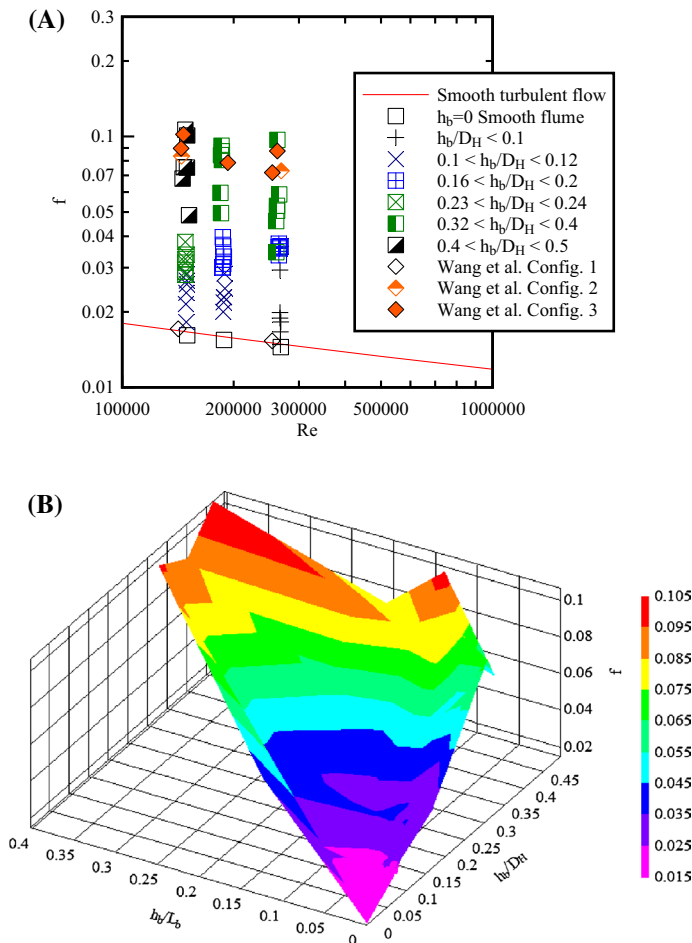
Fig. 5 Flow resistance and Darcy–Weisbach friction factor of triangular corner baffle channels. **A** Darcy–Weisbach friction factor f as a function of the Reynolds number *Re*—comparison with the Karman-Nikuradse formula for smooth turbulent flows and with the data of Wang et al. [43] (Table 1). **B** Darcy–Weisbach friction factor f as a function of relative baffle height h_b/D_H and relative baffle spacing h_b/L_b (present study)

$$f = f' + 0.285 \times \left(\frac{h_b^4}{L_b \times B^2 \times d} \right)^{0.401} \tag{3}$$

where d is the flow depth and f′ is the smooth turbulent flow friction factor calculated using the Karman-Nikuradse formula [9, 38]:

$$\frac{1}{\sqrt{f'}} = 2.0 \times \log_{10} \left(\text{Re} \times \sqrt{f'} \right) - 0.8 \tag{4}$$

In Eq. (3) right handside, the first term relates to the skin friction while the second term is the form drag component, which is a function of the baffle characteristics (i.e. size and

spacing). Equation (3) was compared successfully to the experimental data, with a normalised correlation coefficient of 0.936 and a standard error of 8.54×10^{-4}.

Note that the data (Fig. 5B, Eq. (3)) indicated that the flow resistance decreased with increasing discharge and water depth, towards smooth turbulent flow results ($f \rightarrow f'$) for design flow conditions when $V_{mean} \approx V_c$ and $h_b/d_c \ll 1$. Thus, the small triangular baffles have a negligible impact on the culvert discharge capacity at design flow for the design afflux.

4 Velocity and bed shear stress distributions

4.1 Velocity distributions

Detailed pressure and velocity measurements were conducted with smooth and triangular baffle boundary configurations at more than 220 locations across the flume width, for flow conditions listed in Table 1. All Prandtl–Pitot tube data indicated that the pressure distributions were hydrostatic everywhere, including immediately downstream of baffles. In this section, the longitudinal velocity component data are discussed.

In the smooth channel configuration, the velocity distributions were symmetrical about the channel centreline. In the presence of triangular baffles at the bottom left corner, the flow became asymmetrical, owing to the wake behind each baffle. The velocity field was skewed, with large velocities towards the right half of the channel. The resulting flow motion led to a complicated secondary flow pattern. Immediately downstream of a baffle, the near-wake region was characterised by some negative flow motion close to the bottom left corner (Fig. 6A right, B right). With increasing downstream distance, the left corner flow region remained affected by some slow flow motion. The pattern led to a flow concentration towards the right part of the channel, with a thinner right sidewall boundary layer region, and a slow-velocity region close to the left sidewall (Fig. 6). Typical time-averaged longitudinal velocity contours are illustrated in Fig. 6 for the baffled channel. In Fig. 6, the left graphs correspond to Q = 0.0261 m³/s, h_b = 0.067 m and L_b = 0.67 m, while the right graphs are for Q = 0.0556 m³/s, h_b = 0.133 m and L_b = 1.33 m. From top to bottom, the graphs correspond to X ≈ 0.05, 0.25, 0.5 and 0.75, where X is the relative distance between two successive baffles: X = (x − x_b)/L_b, with x_b the position of the lead baffle. In each contour plot, the left axis corresponds to the smooth right wall and the right axis to the left wall, where the baffles were located. Note the graphs' axis distortion.

A phenomenon of velocity dip was observed. Namely, at a given transverse location, the maximum velocity V_{max} was observed below the free-surface at a vertical elevation $Z_{Vmax}/d < 1$ where d is the local depth of flow. This is seen in Fig. 6. Such a dip in velocity profile was linked to intense secondary motion and transverse momentum exchange [1, 31]. The maximum velocity and its location were found to be functions of the transverse location (Fig. 7). Figure 7 presents experimental observations for one triangular baffle channel configuration, where V_{fs} is the velocity next to the free-surface. In average, the cross-sectional maximum velocity $(V_{max}/V_{mean})_M \approx 1.05$ was observed at about $Z_{Vmax}/d \approx 0.9$ and $Y_{Vmax}/B \approx 0.5$ in the smooth boundary channel. In the triangular baffle channel, the data yielded $(V_{max}/V_{mean})_M \approx 1.33$ at about $Z_{Vmax}/d \approx 0.65$ and $Y_{Vmax}/B \approx 0.26$ in average. Basically the cross-sectional maximum was observed below the free-surface towards the right smooth sidewall in the presence of triangular baffles in the left corner. For a given baffle configuration, the cross-sectional maximum velocity decreased with increasing discharge,
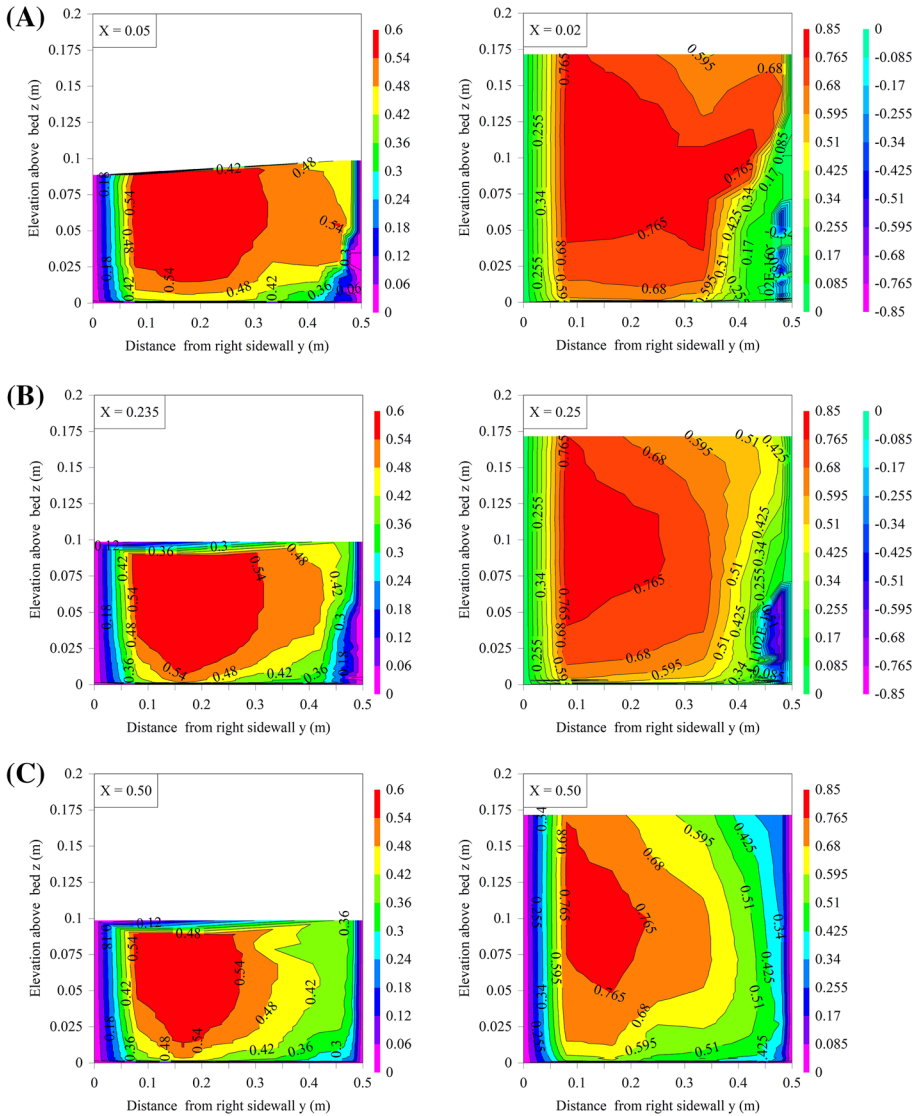
Fig. 6 Contour plots of time-averaged longitudinal velocity V_x (in m/s) looking upstream—left: $Q = 0.0261$ m³/s, $d = 0.121$ m, $h_b = 0.067$ m, $L_b = 0.67$ m, $x_b = 8.12$ m; right: $Q = 0.0556$ m³/s, $d = 0.172$ m, $h_b = 0.133$ m, $L_b = 1.33$ m, $x_b = 8.12$ m—note that, in Fig. 6A (left), negative velocity data were not recorded but labelled $V_x = 0$. **A** $X = 0.05$ and 0.024. **B** $X = 0.235$ and 0.252. **C** $X = 0.50$. **D** $X = 0.765$ and 0.756

while it increased with increasing baffle height for a given discharge and relative baffle spacing. Full results were reported in [4].

The corner baffles induced a significant deceleration of the entire water column close to the left sidewall, within the investigated flow conditions (for $0.44 < h_b/d < 1.3$). The maximum velocity V_{max}/V_{mean} data showed transverse distributions with decreasing values with
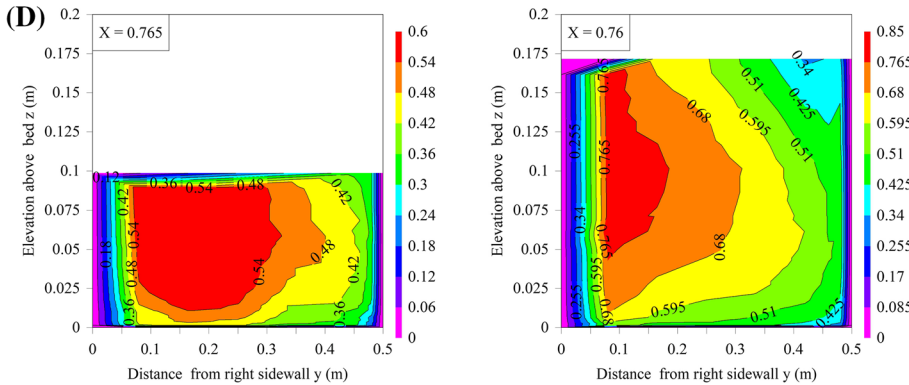
Fig. 6 (continued)

decreasing distance from the triangular baffles (Fig. 7A). The results suggested however that the effects of baffles increased with increasing relative baffle height h_b/d, in particular for $0.5 < h_b/d$. The relative elevation Z_{Vmax}/d of maximum velocity showed a broad scatter in the triangular baffle channel. Next to the left sidewall, the maximum velocity was typically observed at $Z_{Vmax}/h_b \approx 1.1$. It is believed that this corresponded to the region of local fluid acceleration around the baffle and wake separation streamline, as predicted by ideal-fluid flow and free-streamline theory [19, 39]. On the channel centreline ($y/B = 0.5$) of the smooth boundary channel, the ratio of maximum velocity to free-surface velocity V_{max}/V_{fs} equalled 1.01 in average. For comparison, Nezu and Rodi [31] reported $V_{max}/V_{fs} \approx 1.1$ in a smooth and wide channel ($B/d = 10$). In triangular baffle channels, the ratio of maximum velocity to free-surface velocity was consistently larger close to the left sidewall (i.e. triangular baffle wall), with values as large as $V_{max}/V_{fs} \approx 2$.

Within the experimental flow conditions (Table 1), the velocity measurements showed effects of the flow rate and baffle height on the velocity field. For a given baffle configuration, i.e. h_b and L_b constant, a larger discharge Q was associated with a lesser effect of the triangular baffle, in terms of the maximum velocity and its location. Interestingly, the baffle spacing had little effect within the experimental conditions ($L_b/h_b = 5$ and 10). It is believed that a similar flow pattern was observed in all cases, i.e. some baffle-wake interference and interacting flow. The far wake behind each corner baffle interacted with the downstream baffle, and the flow did not fully-recover towards a two-dimensional state before the next triangular baffle element. Such a type of wake interference was documented in flow past strip roughness and rectangular cavities [14, 30, 38].

4.2 Bed shear stress distributions

The skin friction boundary shear stress was measured using the Prandtl–Pitot tube along and across the flume invert. A typical result is shown in Fig. 8, in the form of contour plot of dimensionless skin friction resistance f_{skin}/f on the bed, where f is the overall flow resistance friction factor. It is acknowledged that the data do not include the shear stress distribution on the sidewalls.

For the smooth boundary channel (data not shown), the results showed that the skin friction shear stress was symmetrically distributed about the channel centreline. In the
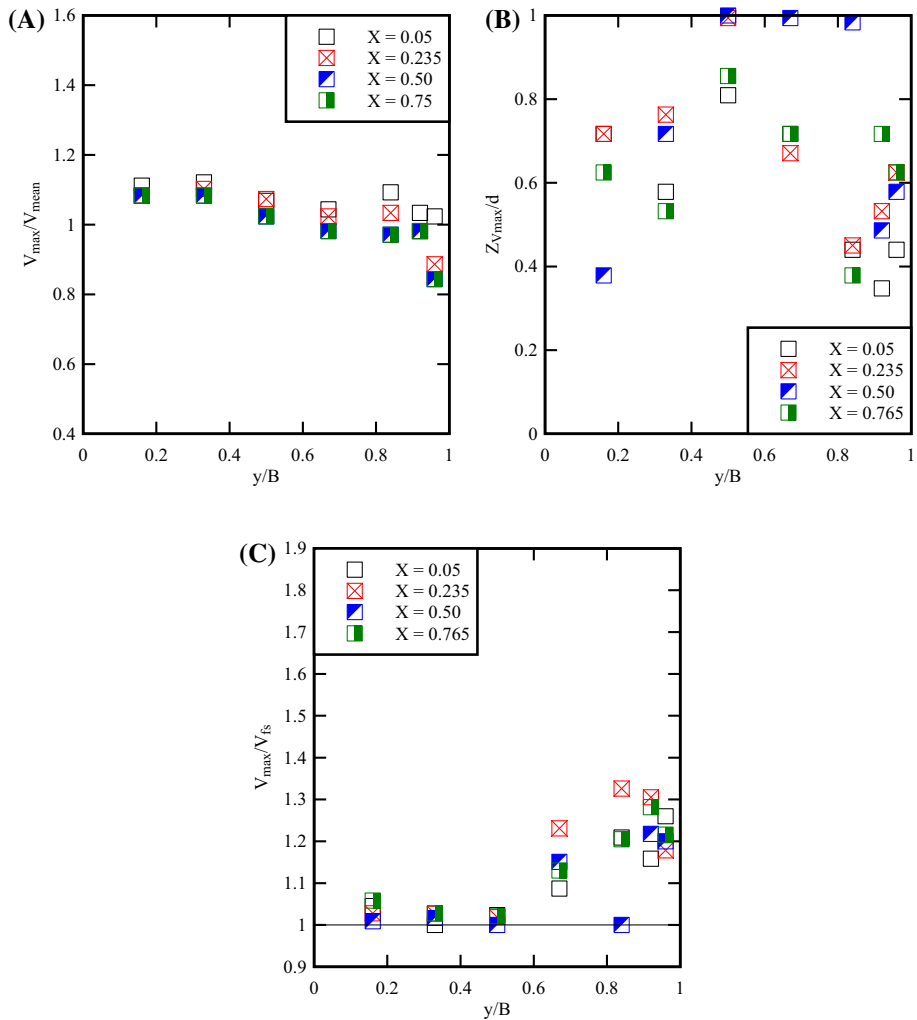
Fig. 7 Transverse distributions of dimensionless maximum velocity V_{max}/V_{mean}, vertical elevation Z_{Vmax}/d and velocity ratio V_{max}/V_{fs}—flow conditions: $Q = 0.0556$ m^3/s, $h_b = 0.067$ m, $L_b = 0.67$ m, $x_b = 8.12$ m. **A**, left Dimensionless maximum velocity V_{max}/V_{mean} as a function of the transverse location y/B. **B**, right Dimensionless vertical elevation Z_{Vmax}/d as a function of the transverse location y/B. **C** Dimensionless velocity ratio V_{max}/V_{fs} as a function of the transverse location y/B

presence of triangular baffles in the left corner, the skin friction shear stress was larger towards the right sidewall (Fig. 8), as a consequence of flow separation behind the baffle and flow concentration towards the right sidewall. Drastically smaller skin friction was recorded towards the left sidewall because of the sheltering effect of the corner baffles.

The results showed further that the skin friction bed shear stress was less than the total boundary shear stress: i.e., $f_{skin}/f < 1$. Since the total boundary shear stress encompassed both skin friction and form drag, the experimental results implied that form drag was sizeable. The skin friction data were spatially-averaged over a longitudinal baffle spacing L_b
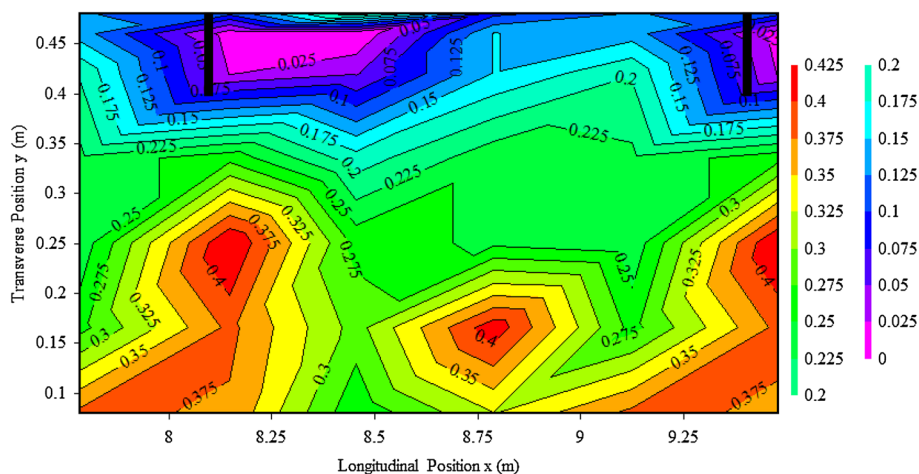
Fig. 8 Contour plot of dimensionless bed boundary shear stress f_{skin}/f in triangular baffle channel—flow direction from left to right, $x_b = 8.12$ m and 9.45 m, $Q = 0.0556$ m³/s, $h_b = 0.133$ m, $L_b = 1.33$ m—solid black lines are triangular baffles ($x_b = 8.12$ and 9.45 m)—legend indicates f_{skin}/f values

Table 2 Spatial-averaged skin friction boundary shear stress in the fully-developed flow in triangular baffle channel ($x_b = 8.12$ m)

Boundary configuration	Baffle height h_b (m)	Baffle spacing L_b (m)	Q (m³/s)	D (m)	V_{mean} (m/s)	f	$<\tau_o>$ (Pa)	$<f_{skin}>$
Smooth	N/A	N/A	0.0261	0.096	0.544	0.0161	–	–
	N/A	N/A	0.0556	0.162	0.686	0.0145	–	–
Baffles	0.067	0.66	0.0261	0.1	0.431	0.0325	0.436	0.0188
	0.067	0.66	0.0556	0.1625	0.684	0.0365	0.599	0.0102
	0.133	0.66	0.0556	0.166	0.643	0.0587	0.660	0.0128
	0.133	1.33	0.0556	0.172	0.647	0.0529	0.674	0.0129

f: dimensionless total boundary shear stress; f_{skin}: dimensionless skin friction boundary shear stress; V_{mean}: cross-section average velocity; τ_o: skin friction boundary shear stress; $<>$: spatial averaging calculated over a baffle spacing L_b

and the channel width. The results are summarised in Table 2. Depending upon the baffle configuration (size, spacing) and flow rate, the ratio of skin friction resistance to total flow resistance f_{skin}/f ranged from 0.21 to 0.58. Basically the skin friction bed shear stress and form drag resistance were of similar magnitude, implying some interplay between skin friction and form drag.

5 Discussion

In a box culvert barrel, there is range of fluid flow velocities, ranging from the cross-sectional maximum water velocity $(V_{max})_M$ to small local velocities V_x close to the boundaries, and $V_x = 0$ at the boundaries. Present results are summarised in Table 3, and compared to

Table 3 Observations of cross-sectional maximum velocities and percentage of wetted cross-section with time-averaged velocity range in the fully-developed flow region (x ~ 8 m)

References	S_o	B (m)	Q (m³/s)	H_b (m)	L_b (m)	D (m)	V_{mean} (m/s)	X	$(V_{max})_M$ (m/s)	% flow area with V_x <		
										V_{mean}	$0.75 \times V_{mean}$	$0.5 \times V_{mean}$
Present study												
Smooth invert	0	0.5	0.0261	N/A	N/A	0.096	0.544	N/A	0.569	70.8	36.4	5.3
			0.0556	N/A	N/A	0.162	0.686	N/A	0.714	72.7	25.9	10.4
Baffles	0	0.5	0.0261	0.067	0.67	0.121	0.431	0.048	0.642	39.6	17.3	14.9
								0.235	0.640	30.5	20.6	14.3
								0.500	0.602	43.7	18.3	12.1
								0.765	0.649	30.7	19.3	10.3
			0.0556	0.067	0.67	0.1625	0.684	0.048	0.767	43.8	20.9	13.5
								0.235	0.754	59.1	24.8	13.8
								0.500	0.774	63.0	22.0	11.5
								0.765	0.741	58.7	31.5	9.7
			0.0556	0.133	0.67	0.173	0.643	0.048	0.858	51.9	26.3	17.5
								0.235	0.861	38.8	22.5	16.6
								0.500	0.817	67.9	31.5	26.1
								0.765	0.835	54.2	28.9	14.4
			0.0261	0.133	1.33	0.1035	0.504	0.048	0.786	35.7	29.9	22.7
								0.235	0.774	44.1	30.5	24.0
								0.500	0.741	55.0	35.1	16.3
								0.765	0.744	48.1	30.7	16.2
Wang et al. [44]												
Rough invert and wall	0	0.4785	0.0261	N/A	N/A	0.129	0.423	N/A	0.755	45	30	17
			0.0556	N/A	N/A	0.1743	0.667	N/A	0.957			

earlier observations by Wang et al. [44] in the same flume, equipped with very-rough invert and left sidewall. The data include the cross-sectional average velocity V_{mean}, the cross-sectional maximum water velocity $(V_{max})_M$, as well as the percentage of flow cross-section area where the time-averaged longitudinal velocity V_x was less than V_{mean}, $0.75 \times V_{mean}$ and $0.50 \times V_{mean}$ (last three columns). In the smooth boundary channel, 5–10% of the flow area experienced time-averaged velocities less than $0.50 \times V_{mean}$. This relative surface area was considerably larger in the triangular baffle channel, with 10–25% of the flow area experiencing $V_x < 0.50 \times V_{mean}$, depending upon the flow rate and baffle configuration.

The presence of triangular baffles increased by a factor two to three the size of slow-flow regions (or low velocity zones). A similar finding was observed by Wang et al. [44] with rough invert and left sidewall. With that configuration, the percentage of the flow area with time-averaged velocities less than $0.50 \times V_{mean}$ was 17%. Such low velocity regions are preferential swimming zones for fish, as shown by Lupandin [26] and Cotel et al. [11]. They are favorable to small-bodied fish passage, because these fish tend to prefer to swim next to sidewalls and flume corners, as shown by fish observations by Wang et al. [43] and Cabonce et al. [4] in the present channel. A key difference between the baffle and rough wall configurations is the longitudinal distribution of the flow. Figure 9 shows photographs of the two configurations side by side. With triangular baffles, flow singularities take place at each baffle, where separation occurs. In the very-rough invert and sidewall configuration, on the other hand, the flow resistance is regularly distributed and flow separation is minimum, typically restricted to the very-near wall region. In the former case, the flow recirculation behind each baffle may provide rest area for small body fish, whereas the latter configuration only provides slow-velocity regions next to the rough boundaries and in the corner regions. Overall the present findings confirmed earlier limited field observations in a box culvert equipped with a different type of corner baffles [37].

The upstream swimming of juvenile silver perch (*Bidyanus bidyanus*) was recorded in the smooth and triangular baffle configuration channel. Tests were conducted with a discharge $Q = 0.0556$ m³/s for up to 17 min with three boundary conditions: (a) smooth channel, (b) medium baffles ($h_b = 0.067$ m, $L_b = 0.67$ m) and (c) large baffles ($h_b = 0.133$ m,
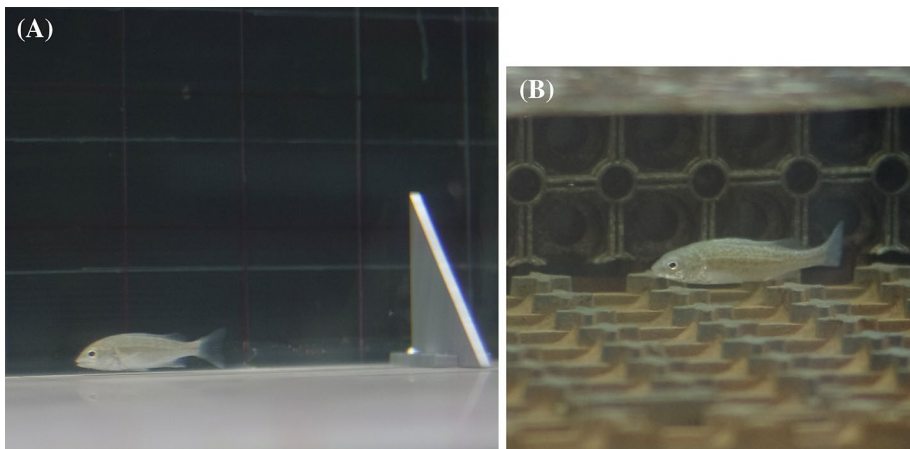

Fig. 9 Photographs of juvenile silver perch (*Bidyanus bidyanus*) swimming upstream in triangular baffle channel [4] and rough boundary channel [43]—flow direction from left to right. **A**, left $Q = 0.0556$ m³/s, triangular baffles: $h_b = 0.067$ m, $L_b = 0.67$ m. **B**, right $Q = 0.0261$ m³/s, rough invert and left sidewall

$L_b = 0.67$ m) (Table 1). Importantly, it must be stressed that the testing was performed with baffle sizes comparable to the fish length. During the tests, a number of fish fatigued before the end of testing: 12 out of 20 with smooth boundaries, 10 out of 26 with medium baffles, and 5 out of 27 with large baffles. The observations showed overall that the presence of triangular baffles allowed fish to rest and facilitated substantially their upstream passage, including in terms of quantitative endurance swim results (Fig. 10). This is illustrated in Fig. 10 showing comparative endurance swim results for all three configurations.

In the smooth channel, the fish tended to swim next to the sidewalls and corners without obvious preference between left and right sidewalls, as previously reported [43]. In the presence of triangular baffles, visual observations showed that the fish swam upstream preferentially in the left corner of the flume, where the triangular baffles were located. Fish were able to pass upstream by taking advantage of the slow-velocity regions, and by resting in the stagnation zone immediately upstream of a baffle or in the wake behind each baffle. Observations and fish trajectory data showed several behaviours [4]. The four dominant upstream swimming patterns included fish resting in the stagnation region immediately upstream of each baffle (Figs. 2B, 9A), fish resting in the near-wake region immediately downstream of baffle, fish progressing upstream along the corner between two adjacent baffles, and fish negotiating the upstream passage of baffle. The most successful upstream

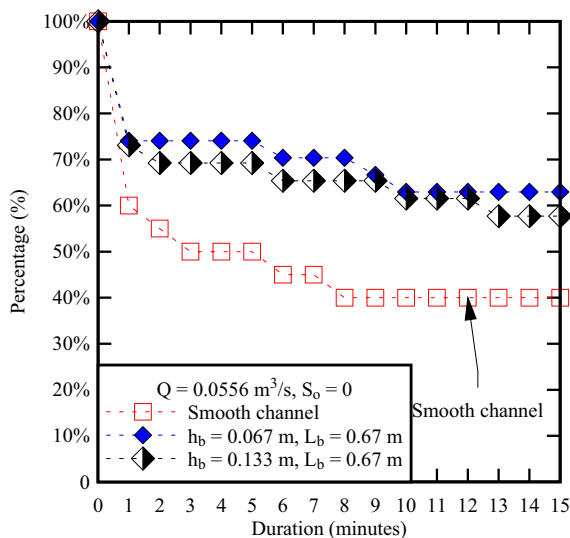| Specie	Boundary conditions	Number tested	Mass median (g)	Mass std dev (g)	Total length median (mm)	Total length std dev (mm)
Juvenile silver perch	Smooth	20	1.5	1.16	53.0	11.8
	Baffle: $h_b = 0.067$ m, $L_b = 0.67$ m	26	1.3	0.85	47.0	9.6
	Baffle: $h_b = 0.133$ m, $L_b = 0.67$ m	27	3.7	2.81	70.5	16.7

Fig. 10 Cumulative test duration data for juvenile silver perch (*Bidyanus bidyanus*) negotiating upstream passage in the 12 m long 0.5 m wide flume: $Q = 0.0556$ m³/s, $S_o = 0$—comparison between three boundary configurations—fish data including fish mass m_f and total length L_f

fish passage technique was observed with fish resting in the stagnation zone upstream of a baffle (illustrated in Fig. 2B), then progressing upstream along the corner, negotiating the upstream baffle by side-stepping the baffle while swimming close to the bed, and then entering the stagnation zone in front of the upstream baffle. During upstream passage, the fish took advantages of the wake interference between baffles, creating a continuous low velocity zone in the left corner where the baffles were installed. Present tests suggested that a longitudinal baffle spacing $L_b/h_b = 5$–10 achieved excellent wake interference regime favourable to the upstream passage of small-bodied fish.

It was noted that a number of fish seemed affected by the flow reversal motion immediately downstream of baffle. These individuals appeared confused by the flow direction, typically facing downstream and were unable to negotiate the upstream passage of the baffle.

Overall the present findings were consistent with the fish trajectory observations of Wang et al. [43] in a rough boundary channel. That is, fish preferred to swim in slow-velocity regions, typically next to the sidewall and in the corner.

6 Conclusion

A small triangular corner baffle system was developed for standard box culvert barrels, producing little reduction in discharge capacity while creating slow flow regions upstream and downstream of baffles. This simple baffle design may assist with the upstream passage of small body mass fish in the barrel of culvert structures on a very flat bed slope, with a baffle size comparable to the targeted fish length ($h_b/L_f \sim 1$). The system was herein tested systematically in a near-full-scale physical facility, for less-than-design flow conditions. The test section was 0.5 m wide and 12 m long, corresponding to a small road culvert structure. The observations indicated several key flow features between successive baffles. In the wake of each baffle, a recirculation region was evidenced with flow reversal. The recirculation region height was about the baffle size h_b, while its length was of the order of three baffle heights ($3 \times h_b$). Further downstream and immediately upstream of the next baffle, a stagnation region was observed, in which the fluid velocity was small and that small-bodied fish used as resting place during upstream passage. The presence of triangular corner baffles had a moderate effect on the flow resistance, albeit the data indicated the combined effect of relative baffle height h_b/D_H and spacing h_b/L_b on the friction factor.

Velocity measurements showed that, with corner baffles, the flow was asymmetrical, with the velocity field showing large velocities towards the smooth sidewall half of the channel, and negative velocities behind the baffles, with complicated velocity distributions next to the left corner. The presence of triangular baffles increased the surface area of slow velocity regions by a factor of two to three. Such low velocity zones are preferential swimming zones for fish and would be beneficial to small-bodied fish passage. In the culvert barrel, the skin friction boundary shear stress was consistently smaller than the total boundary shear stress in the triangular baffle channel. The ratio of skin friction resistance to total flow resistance $(\tau_o)_{skin}/\tau_o$ ranged from 0.21 to 0.58, depending upon the baffle configuration (size, spacing) and flow rate.

Tests with small-bodied fish showed that fish preferred to swim upstream in slow-velocity regions, typically next to the sidewall and in the left corner where the small triangular baffles were located. The presence of triangular baffles facilitated substantially the upstream passage of small fish, for which $L_f/h_b \sim 1$, including in terms of endurance, compared to a smooth un-baffled culvert barrel. A longitudinal baffle spacing $L_b/h_b = 5$–10 appeared to be optimum.

With small-body-mass fish, two unexpected observations were the adverse impact of strong adverse recirculation behind baffles and the most efficient resting location upstream of the baffles. Altogether the present investigation delivered a detailed characterisation of the flow field in smooth and triangular baffle channels, at a scale comparable to a small standard box culvert barrel. It is acknowledged that further tests must be conducted with other species. The present results may provide the relevant data to derive a predictive physically-based model of the flow characteristics of triangular baffle culverts.

Appendix: Theoretical calibration of Prandtl–Pitot tube

A Prandtl–Pitot tube may be used to determine the shear stress at a wall in a turbulent boundary layer [35, 36]. The (skin friction) boundary shear stress is deduced from a calibration curve between the velocity head and the shear stress, when the tube is in contact with the wall. On the basis of the velocity distribution shape, a theoretical calibration may be derived. Herein, V_b is the velocity measured with the Prandtl–Pitot tube lying on the boundary and z_b equals half of the Prandtl–Pitot tube outer diameter. For a turbulent flow, the velocity distribution in the whole boundary layer may be approximated by a power law [2, 17]:

$$\frac{V_x}{V\mathrm{max}} = \left(\frac{z}{\delta}\right)^{1/N} \tag{5}$$

where V_{max} is the free-stream velocity at the outer edge of the boundary layer: $V_{max} = V_x(z = \delta)$, z is the vertical elevation and $N = 7$ for a smooth turbulent boundary layer [25, 38].

In the wall region of a turbulent boundary layer, the Prandtl mixing length may be: $l_m = \kappa \times z$ where κ is the von Karman constant ($\kappa = 0.4$) [9, 38]. At the wall, the boundary shear stress equals:

$$\tau_o = \rho \times \nu_T \times \left(\frac{\partial V_x}{\partial z}\right)_{z=0} = \rho \times l_m^2 \times \left(\frac{\partial V_x}{\partial z}\right)_{z=0}^2 \tag{6}$$

where ν_T is the momentum exchange coefficient or "eddy viscosity". If the velocity distribution follows Eq. (5), the velocity gradient equals:

$$\frac{\partial V_x}{\partial z} = \frac{V_x}{N \times z} \tag{7}$$

and the boundary shear stress becomes:

$$\tau_o = \rho \times \kappa^2 \times \frac{V_b^2}{N^2} \tag{8}$$

Equation (8) gives an expression of the boundary shear stress as a function of the velocity V_b measured with the Prandtl–Pitot tube lying on the boundary. Note that the result is independent of the tube diameter, contrarily to the findings of Patel [35] and Macintosh [27], although Eq. (8) implies that z_b is higher than viscous sub-layer and within the wall region.

References

1. Apelt CG, Xie Q (2011) Measurements of the turbulent velocity field in a non-uniform open channel. In: E Valentine, C Apelt, J Ball, H Chanson, R Cox, R Ettema, G Kuczera, M Lambert, B Melville, J Sargison (eds) Proc. 34th IAHR World Congress, Brisbane, Australia, 26 June–1 July, Engineers Australia Publication, pp 3338–3345. ISBN: 978-0-85825-868-6
2. Barenblatt GI (1994) Scaling, phenomena in fluid mechanics. Inaugural Lecture Delivered before the University of Cambridge on 3 May 1993, Cambridge University Press, UK, 49 pp
3. Behlke CE, Kane DL, McLeen RF, Travis MT (1991) Fundamentals of culvert design for passage of weak-swimming fish. Report FHW A-AK-RD-90-10, Department of Transportation and Public Facilities, State of Alaska, Fairbanks, USA, 178 pp
4. Cabonce J, Fernando R, Wang H, Chanson H (2017) Using Triangular baffles to facilitate upstream fish passage in box culverts: physical modelling. *Hydraulic* Model Report No. CH107/17, School of Civil Engineering, The University of Queensland, Brisbane, Australia, 130 pp
5. Cahoon JE, McMahon T, Solcz A, Blank M, Stein O (2007) Fish passage in Montana Culverts: Phase II—passage goals. Report FHWA/MT-07-010/8181, Montana Department of Transportation and US Department of Transportation, Federal Highway Administration, 61 pp
6. Chanson H (2000) Boundary shear stress measurements in undular flows: application to standing wave bed forms. Water Resour Res 36(10):3063–3076. https://doi.org/10.1029/2000WR900154
7. Chanson H (2002) Hydraulics of a large culvert beneath the Roman aqueduct of Nîmes. J Irrig Drain Eng ASCE 128(5):326–330. https://doi.org/10.1061/(ASCE)0733-9437(2002)128
8. Chanson H (2004) The hydraulics of open channel flow: an introduction, 2 edn. Butterworth-Heinemann, Oxford. ISBN: 978-0-7506-5978-9
9. Chanson H (2014) Applied hydrodynamics: an introduction. CRC Press, Leiden. ISBN: 978-1-138-00093-3
10. Chorda J, Larinier M, Font S (1995) Le Franchissement par les Poissons Migrateurs des Buses et Autres Ouvrages de Rétablissement des Ecoulements Naturels lors des Aménagements Routiers et Autoroutes. Etude Expérimentale. Rapport HYDRE n°159 - GHAAPPE n°95-03, Groupe d'Hydraulique Appliquée aux Aménagements Piscicoles et à la Protection de l'Environnement, Service d'Etudes Techniques des Routes et Autoroutes, Toulouse, France, 116 pp **(in French)**
11. Cotel AJ, Webb PW, Trittico H (2006) Do brown trout choose locations with reduced turbulence? Trans Am Fish Soc 135:610–619
12. Darcy HPG (1858) Note relative à quelques modifications à introduire dans le tube de Pitot. Annales des Ponts et Chaussées XV:351–359 & 1 plate **(in French)**
13. Darrozes SS, Monavon A (2014) Analyse Phénoménologique des Ecoulements. Comment traiter un Problème de Mécanique des Fluides avant de résoudre les Equations. ('Phenomenological Analysis of Flows. How to solve a Fluid Mechanics Problem before solving the Equations.') Presses Polytechniques et Universitaires Romandes, Lausanne, Switzerland, 480 pp **(in French)**
14. Djenidi L, Elavarasan R, Antonia RA (1999) The turbulent boundary layer over transverse square cavities. J Fluid Mech 395:271–294
15. Fairfull S, Witheridge G (2003) Why do fish need to cross the road? Fish passage requirements for waterway crossings. NSW Fisheries, Cronulla NSW, Australia, 14 pp
16. Foss JF, Panton R, Yarin A (2007) Nondimensional representation of the boundary-value problem. In: Tropea C, Yarin AL, Foss JF (eds) Springer handbook of experimental fluid mechanics. Part A, Chapter 2. Springer, pp 33–82
17. George WK (2006) Recent advancements towards the understanding of turbulent boundary layers. AIAA J 44(11):2435–2449
18. Hee M (1969) Hydraulics of culvert design including constant energy concept. In: Proc. 20th Conf. of Local Authority Engineers, Dept. of Local Govt, Queensland, Australia, paper 9, pp 1–27
19. Helmholtz HLF (1868) Über discontinuirliche Flüssigkeits-Bewegungen. Monatsberichte der königlich preussichen Akademie der Wissenschaft zu Berlin, pp 215–228 **(in German)**
20. Henderson FM (1966) Open channel flow. MacMillan Company, New York

21. Herr LA, Bossy HG (1965) Hydraulic charts for the selection of highway culverts. Hydraulic Eng. Circular, US Dept. of Transportation, Federal Highway Admin., HEC No. 5, December
22. Howe JW (1949) Flow measurement. In: Rouse H (ed) Proc 4th Hydraulic Conf., Iowa Institute of Hydraulic Research. Wiley, pp 177–229
23. Hunt M, Clark S, Tkach R (2012) Velocity distributions near the inlet of corrugated steep pipe culverts. Can J Civ Eng 39:1243–1251
24. Larinier M (2002) Fish passage through culverts, rock weirs and estuarine obstructions. Bulletin Français de Pêche et Pisciculture 364(18):119–134
25. Liggett JA (1994) Fluid mechanics. McGraw-Hill, New York
26. Lupandin AI (2005) Effect of flow turbulence on swimming speed of fish. Biol Bull 32(5):461–466
27. Macintosh JC (1990) Hydraulic characteristics in channels of complex cross-section. Ph.D. thesis, University of Queensland, Department of Civil Engineering, Australia, November, 487 pp. https://doi.org/10.14264/uql.2015.218
28. Macintosh JC, Isaacs LT (1992) RPT—The Roving Preston Tube. In: Proc. 11th Australasian Fluid Mechanics Conference, 11AFMC, Hobart, Australia, vol II, Paper 8E-1, pp 1049–1052
29. Monk SK, Wait LE, Hotchkiss RH, Billman E, Belk M, Stuhft D (2012) Culvert roughness elements for native Utah fish passage. In: Proc. World Environmental and Water Resources Congress, ASCE, Albuquerque NM, USA, 20–24 May, pp 1301–1307
30. Morris HM (1955) A new concept of flow in rough conduits. Trans ASCE 120:373–410
31. Nezu I, Rodi W (1985) Experimental study on secondary currents in open channel flow. In: Proceedings 21st IAHR Biennial Congress, Melbourne, Australia, pp 114–119
32. Novak P, Cabelka J (1981) Models in hydraulic engineering. Physical principles and design applications. Pitman Publ., London
33. O'Connor C (1993) Roman bridges. Cambridge University Press, Cambridge
34. Olsen A, Tullis B (2013) Laboratory study of fish passage and discharge capacity in slip-lined, baffled culverts. J Hydraul Eng ASCE 139(4):424–432
35. Patel VC (1965) Calibration of the Preston tube and limitations on its use in pressure gradients. J Fluid Mech 23(Part 1):185–208
36. Preston JH (1954) The determination of turbulent skin friction by means of Pitot tubes. J R Aeronaut Soc Lond 58:109–121
37. Quadrio J (2007) Passage of fish through drainage structures. Queensland Roads, pp 6–17
38. Schlichting H (1979) Boundary layer theory, 7th edn. McGraw-Hill, New York
39. Streeter VL (1948) Fluid dynamics. McGraw-Hill Publications in Aeronautical Science, New York
40. Troskolanski AT (1960) Hydrometry: theory and practice of hydraulic measurements. Pergamon Press, Oxford
41. Wang H, Chanson H (2017) How a better understanding of Fish-Hydrodynamics Interactions might enhance upstream fish passage in culverts. Research Report No. CE162, School of Civil Engineering, The University of Queensland, Brisbane, Australia, 43 pp. ISBN: 978-1-74272-192-7
42. Wang H, Chanson H (2018) Modelling upstream fish passage in standard box culverts: interplay between turbulence, fish kinematics, and energetics. River Res Appl 34(3):244–252. https://doi.org/10.1002/rra.3245
43. Wang H, Chanson H, Kern P, Franklin C (2016) Culvert hydrodynamics to enhance upstream fish passage: fish response to turbulence. In: Ivey G, Zhou T, Jones N, Draper S (eds) Proceedings of 20th Australasian Fluid Mechanics Conference, Australasian Fluid Mechanics Society, Perth WA, Australia, 5–8 December, Paper 682, 4 pp
44. Wang H, Uys W, Chanson H (2018) Alternative mitigation measures for fish passage in standard box culverts: physical modelling. J Hydro-environ Res 19:214–223. https://doi.org/10.1016/j.jher.2017.03.001
45. Webb PW, Cotel AJ (2011) Stability and turbulence. In: Encyclopedia of fish physiology: from genome to environment, vol 1–3. Academic Press, San Diego, pp 581–586. https://doi.org/10.1016/b978-0-12-374553-8.00221-5